Complexation between a Semiflexible Polyelectrolyte and an Oppositely Charged Sphere

Roland R. Netz*,† and Jean-François Joanny‡

Max-Planck-Institut für Kolloid- und Grenzflächenforschung, Am Mühlenberg, 14424 Potsdam, Germany, and Institut Charles Sadron, 6 rue Boussingault, 67083 Strasbourg, France

Received February 23, 1999; Revised Manuscript Received July 26, 1999

ABSTRACT: We study theoretically the interaction of a charged, semiflexible polymer with an oppositely charged sphere. Both the effects of added salt (leading to a finite screening length) and of a bare stiffness of the polymer are taken into account. For intermediate salt concentration and high enough sphere charge we obtain a strongly bound complex where the polymer completely wraps around the sphere. The complex may or may not exhibit charge reversal, depending on the sphere charge and salt concentration. The low-salt regime is dominated by the polymer−polymer repulsion and leads to a characteristic hump shape: the polymer partially wraps around the sphere, and the two polymer arms extend parallel and in opposite directions from the sphere. In the high-salt regime we find bent solutions, where the polymer partially wraps the sphere and the polymer ends extend in arbitrary directions from the sphere; in this regime, the wrapping transition is strongly discontinuous. This wrapping behavior agrees qualitatively well with the salt-induced release of DNA from nucleosomal core particles. The salt dependence of the wrapping transition for large salt concentrations agrees with experimental results for the complexation of synthetic polyelectrolytes with charged micelles. Other applications include the complexation of polyelectrolytes with charged colloids or multivalent ions. In our analysis we calculate the classical or optimal path of the polymer, using a perturbational scheme. This calculation is confirmed and augmented by scaling arguments, which in addition allow us to consider the effect of polymer fluctuations.

I. Introduction

Polyelectrolytes are polymers carrying dissociated ionic groups. They are usually soluble in polar solvents and in most cases in water.[1,2] The long-range character of the electrostatic interactions gives polyelectrolytes very specific properties which are only partially understood from the theoretical point of view.[3] In aqueous solution, polyelectrolyte chains strongly interact with other charged mesoscopic objects, and in particular, they tend to associate with charged objects of opposite sign and form complexes. The complexing agent can be a flexible or a rigid polyelectrolyte, a small colloidal particle, a protein, or a surfactant aggregate such as a micelle or a vesicle.

Complexes formed by polyelectrolytes and a spherical colloidal particle of opposite sign have been experimentally extensively studied recently.[4,5] Apart from being interesting for a variety of applications, they are simple models for the complexation between a polyelectrolyte (such as DNA) and proteins[6] or, more specifically, for histone−DNA complexes in nucleosomal core particles[7−9] and for the interaction between polyelectrolytes and charged surfactant micelles[10] or charged vesicles; in an extreme limit, these complexes can also be viewed as a model for the interaction between a polyelectrolyte and multivalent counterions. Note that these examples are differentiated by the size of the spherical objects which varies over several orders of magnitude.

The polyelectrolyte−sphere complexation has been studied theoretically by various authors who have identified, using more or less realistic models, several important issues. The precise nature of the complex depends on many parameters: the charge of the sphere Z, the linear charge density of the polymer τ, the ionic strength (parametrized by the screening length κ^{-1}), the sphere radius D, the flexibility of the polymer (measured by an intrinsic persistence length l_0). In a series of papers, Wallin and Linse[11] have performed Monte Carlo simulations of polyelectrolytes complexing surfactant micelles; they focus on the so-called critical aggregation concentration at which the surfactant molecules first aggregate in the presence of the polyelectrolyte and vary systematically all the relevant parameters. Marky and Manning[12] have studied complexes between semiflexible polyelectrolytes and rigid spheres using an extremely simplified model for the electrostatic interaction. They show that there can exist a "wrapping transition" between a slightly bent conformation of the polyelectrolyte close to the sphere and a conformation where the polyelectrolyte wraps around the sphere. On the opposite hand, Mateescu et al.[13] ignore the chain stiffness and focus on the electrostatic interactions between the polymer and the sphere at low ionic strength (in the absence of external salt). They show that there is always overcharging of the sphere by adsorption of monomers of opposite sign, in agreement with the simulation results of reference.[11] They also find a "wrapping transition" as the diameter of the sphere is increased, both analytically and by Monte Carlo simulation. Above the transition, the polymer collapses on the sphere. The charge inversion of the sphere by polyelectrolyte adsorption has also been predicted by Park et al.[14] using a Poisson−Boltzmann description of the electrostatic interactions for the adsorption of a semiflexible polyelectrolyte on a cylinder or a sphere and by Gurovitch and Sens,[15] who studied the adsorption of a flexible (Gaussian) weakly charged polyelectrolyte chain on a pointlike sphere.

In this paper we revisit the adsorption of a semiflexible polyelectrolyte chain on a spherical surface of

† Max-Planck-Institut.
‡ Institut Charles Sadron.

10.1021/ma990264+ CCC: $18.00
Published on Web 12/07/1999

opposite charge taking into account on a more detailed level both the electrostatic interaction and the chain stiffness. The attractive electrostatic interaction between the polymer and the sphere can be monitored not only by varying the polymer line-charge density and the sphere charge but also by changing the ionic strength of the solution. It is also known that at least for rigid polyelectrolytes an increase of ionic strength leads to a decrease of the effective stiffness of the chain (the electrostatic persistence length depends on the probed length scale and decreases with ionic strength).[3] The intrinsic stiffness of the chain is another important parameter that is varied. We treat all electrostatic interactions on the Debye−Hückel level; i.e., our results are for polyelectrolyte chains which are above the Manning condensation threshold only accurate for very high salt concentration.[16] The entropy of counterions release is therefore only captured on the linear level. This entropic term has been shown to favor complexation.[14]

In our calculation we perturbatively solve the Euler equation describing the polymer configuration which minimizes the overall energy. Clearly, this (ground-state) approximation is valid only for spheres smaller than the total persistence length of the polymer. For larger spheres, the chain stiffness is less relevant, fluctuations become important, and the results of references[15,17,18] are relevant. In this limit, we include chain fluctuations by augmenting our present calculations with the recently obtained scaling laws for the adsorption of stiff polyelectrolytes on planar charged substrates[16] and thus obtain a complete description of the complexation behavior.

For the resulting sphere−polymer complex we obtain the following three broad classes: For very small sphere charge and very small or large salt concentration, we obtain a weakly deformed polymer which is in contact with the sphere at one point. For intermediate sphere charge and rather low salt concentration, we observe a bent polymer that touches the sphere over a finite segment of its length. For large sphere charge and intermediate salt concentration, the polymer completely wraps around the sphere. Our aim is to construct a phase diagram for the transitions between these various states when the physicochemical parameters are varied.

The paper is organized as follows. In the next section, we present the model describing the polyelectrolyte and the complex and the perturbative approach. In section III, we discuss the complexation phase diagram. The stability of the complex and the possibility of charge inversion are discussed in section IV. The last section presents some concluding remarks and raises some possible issues.

II. Structure and Free Energy of the Polyelectrolyte Complex

A. Complex Free Energy. The complex free energy includes the bending energy of the polymer and the electrostatic interactions between the monomers (repulsive) and between the polymer and the sphere (attractive). We assume here that the reduced electrostatic potential is smaller than unity everywhere and therefore the Debye−Hückel approximation is valid. The polymer is a semiflexible chain of contour length L. In our actual calculation we consider this length as infinite.

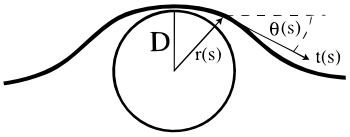

Figure 1. Geometry for the interaction of one semiflexible polymer, parametrized by the contour-length-dependent position $\mathbf{r}(s)$, with one charged sphere of radius D. The contour-length-dependent angle $\theta(s)$ measures the angle the tangent vector $\mathbf{t}(s)$ makes with the tangent vector at the point where the polymer is in contact with the sphere.

The total energy reads

$$\frac{H}{k_B T} = \tau^2 \int_{-L/2}^{L/2} ds \int_s^{L/2} ds' \, v_{pp}(\mathbf{r}[s] - \mathbf{r}[s']) + \frac{l_0}{2} \int_{-L/2}^{L/2} ds \left(\frac{d^2\mathbf{r}[s]}{ds^2}\right)^2 - Z\tau \int_{-L/2}^{L/2} ds \, v_{sp}(\mathbf{r}[s]) \quad (1)$$

The geometry of the complex is depicted in Figure 1. The conformation of the polymer is described by the position $\boldsymbol{r}[s]$ of the monomer whose abscissa along the chain (the contour length) is s. The origin of the contour length is taken at a contact point between the polymer and the sphere. The charged sphere is centered at the origin and has a radius D. We always implicitly assume that a hard core repulsion acts between the sphere and the polymer which enforces $|\mathbf{r}[s]| \geq D$ for all values of s. For the electrostatic repulsion between monomers, we use the standard Debye−Hückel potential,

$$v_{pp}(\mathbf{r}) = \frac{l_B}{r} e^{-\kappa r} \quad (2)$$

where the so-called Bjerrum length $l_B \equiv e^2/(4\pi\epsilon k_B T)$ measures the separation at which the interaction between two elementary charges is of the order of the thermal energy. In water, $l_B \approx 0.7$ nm. The screening length κ^{-1} is determined by the salt concentration c; $\kappa^2 = 8\pi l_B c$ for monovalent salt. There are modifications to the polymer−polymer interaction due to image-charge effects associated with the low-dielectric constant of the sphere and due to the impenetrability of the sphere for salt ions. These effects are important only for large spheres with $D > \kappa^{-1}$ and will be taken into account at the proper place. For the electrostatic sphere−polymer interaction we use the Debye−Hückel approximation with a constant charge boundary condition,[19]

$$v_{sp}(\mathbf{r}) = \frac{l_B}{r(1 + D\kappa)} e^{-\kappa(r-D)} \quad (3)$$

For a sphere much smaller than the screening length, $\kappa D \ll 1$, the two expressions eqs 2 and 3 are essentially identical; on the other hand, for a sphere much larger than the screening length, $\kappa D \gg 1$, curvature effects become negligible close to the sphere surface and the sphere−polymer interaction goes over to the Debye−Hückel potential of a plane with surface charge density $Z/(4\pi D^2)$. The stiffness of the polymer is described by a Krattky−Porod model with a bare persistence length l_0; we also assume the polymer to have a conserved length, i.e. $|d\mathbf{r}[s]/ds| = 1$.

B. Perturbative Approach. Our aim in this paper is to determine the structure of the complex by minimization of its free energy i.e. to find the *ground state* of the free energy eq 1. This ground state arises from a competition between the self-energy of the polymer, the

first two terms in eq 1, which favor a straight polymer conformation, and the sphere−polymer attraction, the third term in eq 1, which tends to bring the polymer close to the sphere surface and thus favors a wrapping of the polymer around the sphere. In principle, the ground state follows from eq 1 using a variational procedure, leading to an Euler equation. The Euler equation can be written down explicitly, but the solution proves prohibitively difficult. We therefore resort to a perturbative analysis, similar in spirit to a method which has been introduced to study the persistence length of a charged rod[20] and the mutual interaction of rigid polyelectrolytes in solution.[21] In the following we also restrict ourselves to polymer configurations which lie in a common plane with the sphere center. This is certainly a good approximation if the polymer remains weakly bent. If the polymer wraps around the sphere, its conformation is clearly three-dimensional. In this case we augment this two-dimensional description by a scaling analysis which properly takes into account the third dimension.

A convenient variable to parametrize the polymer is the local curvature of the chain, $\dot{\theta}(s)$, which is given by the derivative of the angle between the local tangent to the chain and a given direction; it determines the polymer shape up to one rotational angle. The angle offset is imposed by defining the angle at closest approach to be zero, as depicted in Figure 1. In a systematic expansion around the totally stretched polymer configuration, $\dot{\theta}(s) = 0$ everywhere, the energy difference can (up to second order in $\dot{\theta}(s)$) be written as

$$\frac{\Delta H}{k_B T} = \frac{1}{2}\int_{-L/2}^{L/2} ds \int_{-L/2}^{L/2} ds'\, \dot{\theta}(s)\dot{\theta}(s')[K(s,s') + l_0\delta(s-s')] - \int_{-L/2}^{L/2} ds\, \dot{\theta}(s) g(s) \quad (4)$$

The kernel $K(s,s')$ is given by

$$K(s,s') = \tau^2 \int_{-L/2}^{s'} ds_1 \int_{s}^{L/2} ds_2\, v'_{pp}(s_2 - s_1) \times \frac{(s_2 - s)(s' - s_1)}{|s_2 - s_1|} \quad (5)$$

We use here the kernel obtained for a semiflexible polyelectrolyte in the bulk.[20,21] As mentioned before, the interactions between monomers in the vicinity of the adsorbing sphere differ from the standard Debye−Hückel law eq 2 because of the dielectric discontinuity introduced by the dielectric sphere and because the salt ions cannot penetrate the sphere. These two effects are extremely difficult to treat quantitatively. When the dielectric constant of the sphere is much smaller than the dielectric constant of water, these two effects do not modify the scaling structure of the kernel K although they may in certain cases change the numerical prefactors. In the following we work mostly at the scaling level and postpone these delicate points to the scaling discussion of image-charge effects in section IV. The function $g(s)$ reads

$$g(s) = -\tau Z D \int_s^\infty ds' \frac{v'_{sp}(\sqrt{D^2 + s'^2})(s' - s)}{\sqrt{D^2 + s'^2}} \quad (6)$$

The energy of the unperturbed state, i.e. the straight polymer which just touches the sphere at one point, is given by (in the limit of an infinitely long polymer)

$$\frac{H_0}{k_B T} = -\frac{Z\tau l_B e^{D\kappa}}{1 + D\kappa}\int_{-\infty}^{\infty} ds\, \frac{e^{-\kappa\sqrt{s^2+D^2}}}{\sqrt{s^2 + D^2}} = -\frac{2Z\tau l_B e^{D\kappa}}{1 + D\kappa} K_0[D\kappa] \quad (7)$$

where K_0 denotes a Bessel function. In the limit of an infinitely long polymer, $L \to \infty$, the kernel eq 5 becomes a function of the contour-length difference $t = s - s'$ only,

$$K(t) = \frac{\tau^2}{6}\int_0^\infty ds\, \frac{s^3}{s + t} v'_{pp}(t + s) \quad (8)$$

In the same limit, $L \to \infty$, we can diagonalize the free energy eq 4 by introducing the Fourier variable ω conjugate to the contour length s and by expressing the free energy in terms of the Fourier components of the curvature,

$$\frac{\Delta H}{k_B T} = \frac{1}{2}\int \frac{d\omega}{2\pi} \tilde{\dot{\theta}}(\omega)\tilde{\dot{\theta}}(-\omega)[\tilde{K}(\omega) + l_0] - \int \frac{d\omega}{2\pi} \tilde{\dot{\theta}}(\omega)\tilde{g}(\omega) \quad (9)$$

The equilibrium curvature obtains from the Euler equation, $\delta\Delta H / \delta\tilde{\dot{\theta}}(\omega) = 0$,

$$\tilde{\dot{\theta}}(\omega) = \frac{\tilde{g}(\omega)}{\tilde{K}(\omega) + l_0} \quad (10)$$

The Fourier transformed kernel $\tilde{K}(\omega) = \int ds\, e^{-i\omega s} K(s)$ can be computed in closed form,

$$\tilde{K}(\omega) = 2l_{OSF}\kappa^2\omega^{-2}[(1 + \kappa^2\omega^{-2}) \ln(1 + \kappa^{-2}\omega^2) - 1] \quad (11)$$

where l_{OSF} denotes the (Odijk−Skolnick−Fixman) electrostatic persistence length: $l_{OSF} = l_B\tau^2\kappa^{-2}/4$. The Fourier transform of the kernel $\tilde{K}(\omega)$ gives the effective scale dependent persistent length at a scale $s \simeq 1/\omega$. In the rest of the paper, we assume that the Odijk−Skolnick−Fixman description of a polyelectrolyte chain remains valid. According to ref 20, this requires that the polyelectrolyte is stiff enough, $l_0 \gg 1/(\tau^2 l_B)$. The Fourier transform of $g(s)$, denoted $\tilde{g}(\omega)$, is calculated in Appendix A.

The two important geometrical characteristics of the complex are the curvature at the origin, $\dot{\theta}_0 \equiv \dot{\theta}(0)$,

$$\dot{\theta}_0 = \int \frac{d\omega}{2\pi} \frac{\tilde{g}(\omega)}{\tilde{K}(\omega) + l_0} \quad (12)$$

and the asymptotic angle infinitely far away from the sphere, $\theta_\infty \equiv \theta(\infty)$,

$$\theta_\infty = \frac{\tilde{g}(0)}{\tilde{K}(0) + l_0} \quad (13)$$

Note that neglecting polymer shape fluctuations around the classical (or optimal) path is only appropriate to describe the polymer conformation at length scales smaller than the persistence length. Above this length scale, angular fluctuations will become dominant. We

also ignore the fact that the polymer chain can fold back on the sphere as shown for example in the simulations of Wallin and Linse.[11] We therefore exclude at this point the case where the radius D of the sphere is larger than the polymer persistence length. This is done later in section IV using scaling arguments. A meaningful interpretation for the angle θ_∞ is that it measures the polymer angle at a distance from the sphere smaller than the total persistence length, such that the polymer is not yet crumpling, but at a distance larger than the electrostatic screening length, such that this angle has saturated and reached its asymptotic value. Neglecting three-body (and higher-order) coupling terms in the perturbative expression eq 4 is an approximation which is hard to judge within the perturbational approach. We should say that the two-body term included in eq 4 captures curvature effects to all orders (for example multiple gradient terms), since the kernel $K(s, s')$ is used in its exact form. There is hope that the approximations involved are quite good, since the wrapping transitions inferred from eq 4 coincide with results from simple, but robust, scaling calculations done in section IV. Additional support comes from recent numerical calculations, where the ground state of the energy expression eq 1 has been determined directly, demonstrating excellent agreement with our perturbative results.[22]

C. Chain Curvature at the Origin. The previous description ignores the impenetrability of the sphere and may lead to a curvature of the polymer chain at the origin larger than the sphere curvature $1/D$. In the (formal) limit of vanishing bare bending rigidity, i.e., for $l_0 = 0$, it follows from eqs 11, A24, and A25 that the integrand in eq 12 decays for large momenta as $\sim 1/\ln(\omega)$ and thus yields an ultraviolet divergence. The polymer forms a kink at the origin and thus violates the impenetrability of the sphere. In the following we introduce a simple method of fixing the curvature at the origin and thus imposing the impenetrability of the sphere. We add a term to the free energy which couples to the curvature at the origin. To obtain an equilibrium curvature at the origin, we also need to add a higher-order elastic term, which regularizes the functional. The additional energy contribution reads

$$\frac{H'}{k_B T} = \frac{m}{2}\int_{-L/2}^{L/2} \mathrm{d}s\, \ddot{\theta}^2(s) - h\dot{\theta}(0) \tag{14}$$

The Euler equation, which follows from the variation $\delta(\Delta H + H')/\delta\tilde{\theta}(\omega) = 0$, is

$$\tilde{\theta}(\omega) = \frac{\tilde{g}(\omega) + h}{\tilde{K}(\omega) + l_0 + m\omega^2} \tag{15}$$

The resulting expressions for the curvature at the origin and the asymptotic angle are

$$\dot{\theta}_0 = \int \frac{\mathrm{d}\omega}{2\pi} \frac{\tilde{g}(\omega) + h}{\tilde{K}(\omega) + l_0 + m\omega^2} \tag{16}$$

and

$$\theta_\infty = \frac{\tilde{g}(0) + h}{\tilde{K}(0) + l_0} \tag{17}$$

The curvature at the origin can be adjusted by tuning h and m, as will be detailed in the following sections.

III. Complexation Behavior

In this section we consider the three possible states of the complex which are found when the charge of the sphere or the salt concentration is changed: polymer being in contact with the sphere only at a point, polymer touching the sphere by a finite length, and polymer wrapping completely around the sphere. In the following we study the transitions between these three states, which are the *touching transition* and the *wrapping transition*.

A. Touching Transition. When the sphere charge is low, the polymer only slightly bends and is in contact with the sphere only at one point. In this point-contact conformation the impenetrability constraint is not important and can be ignored. The conformation of the chain thus follows directly from eq 10, and the curvature at the point of contact is given by eq 12. As the charge of the sphere increases, the polymer curvature at the origin also increases. At some threshold value of the sphere charge, it becomes equal to the sphere curvature. Beyond this point, a finite segment of the chain touches the sphere. Our criterion for the touching transition is thus $\dot{\theta}_0 = 1/D$. The determination of the polymer curvature at the origin is rather technical, and the expressions of the necessary integrals are given in appendices A and B; we now discuss the results for various values of the parameters.

1. Small Bare Bending Rigidity, $1/l_B\tau^2 < l_0 < l_B D^2\tau^2$. We define the rescaled bare bending rigidity,

$$\bar{l_0} \equiv \frac{l_0}{l_B D^2 \tau^2} \tag{18}$$

With this definition, the regime of small bare bending rigidity corresponds to $1/\tau^4 l_B^2 D^2 < \bar{l_0} < 1$.

i. Small Spheres, $D \ll \kappa^{-1}$. In this limit the polymer curvature at the origin, $\dot{\theta}_0$, is calculated in Appendix B.3 and is given by eq B18. For small sphere charge Z the polymer curvature is indeed smaller than the sphere curvature $1/D$. The sphere charge at which the polymer and the sphere curvature are equal, $\dot{\theta}_0$, which determines the touching transition, is

$$Z_t \sim \tau D\left[\bar{l_0} \ln\left(\frac{1}{\bar{l_0} D^2 \kappa^2}\right)\right]^{1/2} \tag{19}$$

For $Z < Z_t$, the polymer contacts the sphere only at one point; for $Z > Z_t$, on the other hand, it touches the sphere over a finite length.

ii. Large Spheres, $D \gg \kappa^{-1}$. For larger spheres or, equivalently, for large salt concentrations, the polymer curvature at the origin exhibits different scaling regimes, depending on the ionic strength (or the screening length). We find three asymptotic regimes separated by the characteristic inverse screening lengths κ_{**} and κ_{***}. At

$$\kappa_{**} \equiv \frac{1}{D\bar{l_0}^{1/2}} \tag{20}$$

the electrostatic persistence length equals the bare persistence length, i.e., we have $l_0 = l_{OSF}$, and κ_{***} is

defined as

$$\kappa_{***} \equiv \frac{1}{D(\bar{l_0} \ln \bar{l_0}^{-1})^{1/3}} \tag{21}$$

In the regime of small bare bending rigidity, $\bar{l_0} < 1$, we always have $\kappa_{***} < \kappa_{**}$. For $D^{-1} < \kappa < \kappa_{***}$ the polymer curvature at the origin is according to eq B29 given by $\dot{\theta}_0 \sim Z\tau^{-1}D^{-2}[\bar{l_0}D\kappa \ln(1/\bar{l_0}\kappa^2D^2)]^{-1/2}$. Therefrom, the touching transition is

$$Z_t \sim \tau D\left[\bar{l_0}D\kappa \ln\left(\frac{1}{\bar{l_0}\kappa^2D^2}\right)\right]^{1/2} \tag{22}$$

The value of Z_t grows with increasing κ. For $\kappa_{***} < \kappa < \kappa_{**}$ eq B29 predicts $\dot{\theta}_0 \sim Z\kappa/\tau D$ and thus the touching transition occurs at

$$Z_t \sim \frac{\tau}{\kappa} \tag{23}$$

Finally, for $\kappa_{**} < \kappa$, corresponding to a bare bending rigidity which is larger than the electrostatic persistence length, eq B30 predicts a curvature at the origin $\dot{\theta}_0 \sim Z/\bar{l_0}\tau\kappa D^3$. This yields a touching transition for a charge

$$Z_t \sim \bar{l_0}\kappa\tau D^2 \tag{24}$$

2. Large Bare Bending Rigidity, $l_0 > l_B D^2\tau^2$. The regime of large bare bending rigidity corresponds to $\bar{l_0} > 1$.

i. Large Spheres, $D \gg \kappa^{-1}$. In this limit the results obtained in the previous section for $\kappa > \kappa_{**}$ are still valid. Specifically, the touching transition is in agreement with eq 24 given by $Z_t \sim \bar{l_0}\kappa\tau D^2$.

ii. Small Spheres, $D \ll \kappa^{-1}$. In this regime the polymer curvature at the origin shows various asymptotic behaviors according to the value of the screening length; we find another characteristic inverse screening length, namely

$$\kappa_* \equiv D^{-1}e^{-\bar{l_0}/2} \tag{25}$$

For $\kappa < \kappa_*$ the results of the previous section obtained for $\kappa < D^{-1}$ are valid and the touching transition is given by eq 19. Note that κ_* is exponentially small and that this regime can in practice be ignored.

In the whole range $\kappa_* < \kappa < D^{-1}$ the polymer curvature at the origin is according to eqs B22 and B26 given by $\dot{\theta}_0 \sim Z/\tau D^2\bar{l_0}$ leading to a touching transition for

$$Z_t \sim \tau D\bar{l_0} \tag{26}$$

The touching transition is independent of the salt concentration.

B. Wrapping Transition. When the sphere charge is higher than the threshold value Z_t, i.e. when the polymer touches the sphere over a finite length, the impenetrability constraint must be taken into account along the lines described in section II.C. To that end, we supplement the perturbative energy expression eq 4 by eq 14 which contains terms proportional to the constants h and m which will be tuned in order to obtain a finite curvature at the origin. The magnitude of h and m can be conveniently described by the crossover scale ω_* at which h and m dominate the integrand in eq 16. Since both $\tilde{g}(\omega)$ and $\tilde{K}(\omega)$ decay to zero for large values of ω, it follows that h and m dominate for large values of ω, i.e., for small spatial scales. The crossover scale ω_* measures the spatial extent up to which the hard-core repulsion of the sphere is felt by the polymer, in other words, the length over which the polymer *touches the sphere*. With this interpretation, it follows that the crossover momentum ω_* should be the same in the numerator and denominator of eq 16 and, thus, is determined by the equations

$$\tilde{g}(\omega_*) = h\tilde{K}(\omega_*) = m{\omega_*}^2 \tag{27}$$

The length and the arc length over which the polymer touches the sphere scale as $l_t \sim {\omega_*}^{-1}$ and $\theta_t \sim {\omega_*}^{-1}D^{-1}$. We consider that the polymer completely wraps around the sphere when the length of the polymer segment in contact with the sphere l_t is of the order of the sphere radius D or equivalently when the angle θ_t over which the polymer bends in contact with the sphere is of order unity. The wrapping transition is therefore defined by $\omega_* \simeq D^{-1}$. An important observable which characterizes the polymer shape is the asymptotic deflection angle, which is according to eq 17 given by

$$\theta_\infty = \frac{Z\tau D l_B e^{\kappa D}K_0(\kappa D)(1+\kappa D)^{-1} + h}{l_{OSF} + l_0} \tag{28}$$

1. Small Bare Bending Rigidity, $1/l_B\tau^2 < l_0 < l_B D^2\tau^2$.

i. Small Spheres, $D < \kappa^{-1}$. The polymer curvature at the origin in the presence of constraints regulating this curvature is given in eq B8. If $\dot{\theta}_0 \sim 1/D$ is enforced, the wrapping threshold, i.e. the sphere charge where the touching length equals the sphere radius, $\omega_* \simeq D^{-1}$, is given by

$$Z_w \sim \tau D \ln\left(\frac{1}{D\kappa}\right) \tag{29}$$

In the limit $\kappa < \kappa_{**}$ the bare stiffness is smaller than the electrostatic persistence length, $l_0 \ll l_{OSF}$, and thus eq 28 reduces to $\theta_\infty \sim ZD\kappa^2\tau^{-1}\ln(1/D\kappa)$. In obtaining this result, we used the fact that the constant h which fixes the curvature at the origin is smaller than $\tilde{g}(0)$ and thus does not influence θ_∞. At the wrapping threshold, $Z \sim Z_w$, the asymptotic angle is given by

$$\theta_{\infty,w} \sim D^2\kappa^2 \ln^2\left(\frac{1}{D\kappa}\right) \tag{30}$$

and is thus much smaller than unity. The typical complex configuration for $D \ll \kappa^{-1}$ close to the wrapping threshold shows a characteristic *hump shape*, as schematically depicted in Figure 2a.

The wrapping transition eq 29 can also be obtained with a more intuitive argument, which we present now. To that end consider the polymer configuration in Figure 3a *before complexation* (which is the reference state) and the configuration in Figure 3b *after complexation*. We assume here that the distance between the polymer and the charge center, R (in this section we identify R with the sphere radius D; later we will also encounter a case where $R > D$), is much smaller than the screening length. The electrostatic energy gained in wrapping the polymer once around the central charge is $f_{att} \sim -l_B Z\tau$. The repulsive energy associated with the increase in electrostatic self-energy of the polymer is calculated in Appendix C and reads $f_{rep} \sim l_B\tau^2 R \ln(1/R\kappa)$. Interestingly, this repulsive energy is mainly

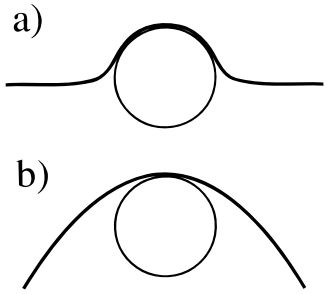

Figure 2. Typical polymer configurations obtained at a sphere charge Z smaller than the threshold for complete wrapping. (a) Hump configuration, obtained for small salt concentration with a screening length κ^{-1} much larger than the sphere radius D. The polymer is locally attracted to the sphere surface, but the repulsion between the two arms leads to a flattening out as one moves away from the sphere. (b) Bent configuration, obtained for large salt concentrations with a screening length smaller than the sphere radius. Here the attraction to the sphere keeps bending the polymer toward the sphere even when the separation from the sphere surface is of the order of the sphere radius.

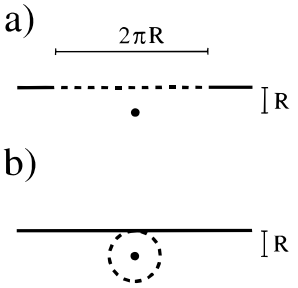

Figure 3. Simplified polymer configurations used to estimate the scaling form of the polymer self-energy in the (a) point contact configuration and in the (b) wrapped configuration.

associated with the repulsion between the two straight arm sections drawn as solid lines in Figure 3, which are pulled closer together. Clearly, this effect is restricted to the case where the screening length is much larger than the wrapping radius R and also to the case where the total length of the polymer exceeds the screening length. The wrapping threshold is within this simple model obtained as the value of the central charge Z at which the attractive energy is larger than the repulsive one, which means $f_{rep} + f_{att} = 0$, and reads

$$Z_w \sim \tau R \ln\left(\frac{1}{R\kappa}\right) \tag{31}$$

Assuming that the polymer touches the sphere, which means $R = D$, we obtain the wrapping threshold eq 29.

We note that the case of no salt, which for example has been considered by Mateescu et al.,[13] is within our approach a singular limit, where our scaling arguments leading to eq 31 or eq 29 are only valid if the polymer length is infinite. However, it turns out that the case of a polymer which is shorter than the screening length can be mapped on the calculation outlined in the preceding section if one assumes that the effective screening length is given by the polymer length, $\kappa^{-1} \simeq L$. One then sees that the wrapping threshold eq 31 becomes $Z_w \sim \tau D \ln(L/R)$. This means that an unwrapping can be induced, even in the case of no screening, by increasing the length of the polymer.

ii. Large Sphere, $D \gg \kappa^{-1}$. We now study the wrapping of a sphere *larger* than the screening length, which is markedly different from that of a sphere *smaller* than κ^{-1}. Above the touching transition, the polymer curvature $\dot{\theta}_0$ at the origin is determined by the curvature constraints which are adjusted such as to fix this curvature at the value of the sphere curvature. According to eq B13 we have

$$\dot{\theta}_0 \sim \frac{Z\kappa}{D\tau}\left(1 + \frac{\omega_*}{D^{1/2}\kappa^{3/2}\ln(\omega_*\kappa^{-1})}\right) \tag{32}$$

Since the sum of the two terms in the parentheses of eq 32 cannot become smaller than unity, there is an upper value of Z up to which the curvature at the origin can be fixed at $\dot{\theta}_0 \sim 1/D$. As follows from eq 32, and as further substantiated below, this stability limit corresponds to the wrapping transition and is given by

$$Z_w \sim \frac{\tau}{\kappa} \tag{33}$$

At the touching transition, that is for $Z \sim Z_w$, the two terms in parentheses in eq 32 scale similarly and we have $\omega_* \sim D^{1/2}\kappa^{3/2}\ln(\omega_*\kappa^{-1})$. The touching length at the wrapping transition is thus given by $l_t \sim \omega_*^{-1} \sim \kappa^{-3/2}D^{-1/2}/\ln(D\kappa)$. Since $\kappa D \gg 1$, l_t is smaller than the screening length. $Z_w \sim \tau/\kappa$ therefore corresponds to a strongly discontinuous wrapping transition, at which the touching length jumps from a value smaller than the screening length to a value corresponding to the sphere radius. The deflection angle at the point where the polymer stops touching the sphere is at the wrapping threshold given by $\theta_t \sim l_t/D \sim \kappa^{-3/2}D^{-3/2}/\ln(D\kappa)$. The asymptotic angle θ_∞ is according to eq 28 for $D\kappa > 1$ and $l_0 < l_{OSF}$ given by $\theta_\infty \sim Z\kappa^{1/2}\tau^{-1}D^{-1/2}$ (the constant h used to fix the curvature at the origin is irrelevant in the calculation of θ_∞). At the wrapping threshold, $Z \sim Z_w$, the asymptotic angle is given by $\theta_\infty \sim \kappa^{-1/2}D^{-1/2}$ and thus much smaller than unity. By comparing the deflection angle where the polymer stops touching the sphere with the angle asymptotically far away from the sphere, we find $\theta_t \ll \theta_\infty \ll 1$ at the wrapping transition; i.e., the polymer bends *toward* the sphere even when it does not touch the sphere. This is different from the result for $D \ll \kappa^{-1}$, where the polymer bends *away* from the sphere when it stops touching the sphere. The typical structure of the complex for $D > \kappa^{-1}$ below the wrapping threshold shows a characteristic *deflection shape*, as depicted schematically in Figure 2b.

The wrapping instability, eq 33, can also be obtained from the following simple scaling argument: for $\tau^2 l_B l_0 > 1$, which we always assume to be true, and for a bending radius D larger than the screening length, the effective persistence length for a deformation at the scale of the sphere radius is the sum of the electrostatic persistence length l_{OSF} and the bare persistence length. The bending energy per unit length is thus $f_{bend} \sim (l_0 + l_{OSF})/D^2$. The electrostatic adsorption energy for a polymer on a sphere surface per unit length is, according to eq 3, given by $f_{ads} \sim -\tau l_B Z\kappa^{-1}D^{-2}$. The wrapping instability is expected when the total energy becomes negative, i.e., for $f_{bend} + f_{ads} \simeq 0$, which leads to

$$Z_w \sim \frac{\kappa}{l_B\tau}(l_0 + l_{OSF}) \tag{34}$$

independently of the sphere radius D. In the limit $l_{OSF} > l_0$, one obtains with $l_{OSF} \sim l_B\tau^2\kappa^{-2}$ the previous result, eq 33. For $l_{OSF} < l_0$ or $\kappa > \kappa_{**}$, on the other hand, we

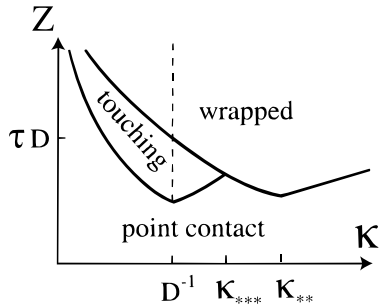

Figure 4. Complete complexation phase diagram for small bare bending rigidity $l_0 < l_B D^2\tau^2$, shown as a function of the sphere charge Z and the inverse screening length κ. Shown are the touching transition, where the polymer starts touching the sphere over a finite contour length, and the wrapping transition, where the polymer completely wraps the sphere. The wrapping transition is strongly discontinuous when it goes directly from a point-contact phase to the wrapped phase, i.e., for high salt concentrations. The dotted line separates the hump from the bent configurations.

obtain from eq 34 the wrapping threshold

$$Z_w \sim \frac{l_0\kappa}{\tau l_B} \sim \bar{l_0}\kappa\tau D^2 \tag{35}$$

The scaling of this wrapping threshold is the same as found experimentally for the complexation of synthetic polyelectrolytes with charged micelles.[10] Also, in this respect, it is interesting to note that the wrapping threshold eq 35 has been determined on more general grounds not using any specific interaction model.[23,24] The complete complexation diagram of a sphere by a polymer of low bending rigidity, defined by $l_0 < l_B D^2\tau^2$, is displayed in Figure 4, containing the touching transition determined by eqs 19, 22, 23, and 24 and the wrapping transition determined by eqs 29, 33, and 35. Note that if $\kappa \gg \kappa_{***}$ the wrapping transition coincides with the touching transition. For $\kappa \gg \kappa_{***}$ we therefore do not find a touching phase where the polymer touches the sphere only on a small segment smaller than the sphere radius. The wrapping transition for high enough salt concentrations is thus strongly discontinuous. The broken line denotes the scaling boundary between a polymer showing the typical hump shape shown in Figure 2a, realized for low screening $\kappa < D^{-1}$, and a polymer showing a bent shape, as shown in Figure 2b.

2. Large Bare Bending Rigidity, $l_0 > l_B D^2\tau^2$. i. Low Salt, $\kappa < \kappa_*$. In this case the analysis leading to the result eq 29 is valid. Comparing the wrapping transition Z_w, eq 29, with the touching transition Z_t, eq 19, we find $Z_t < Z_w$ for $\kappa < \kappa_*$. However, for $\kappa = \kappa_*$ the two transitions meet.

ii. Intermediate Salt, $\kappa_* < \kappa < \kappa_{**}$. In this regime we actually find a loosely wrapped phase, or in other words, the wrapping threshold occurs at a smaller sphere charge than the touching transition. To see this, we note that the bending radius of the polymer at the origin, R, is, according to $R \sim 1/\dot{\theta}_0$ and using the result eq B22 (which is valid below the touching transition), given as

$$R \sim \frac{\tau D^2 \bar{l_0}}{Z} \tag{36}$$

Combining this result for the preferred bending radius of the polymer with the scaling result for the wrapping threshold in the limit of low salt ($R\kappa < 1$) eq 31, we obtain

$$Z_w \sim \tau D\left[\bar{l_0}\ln\left(\frac{1}{\bar{l_0}D^2\kappa^2}\right)\right]^{1/2} \tag{37}$$

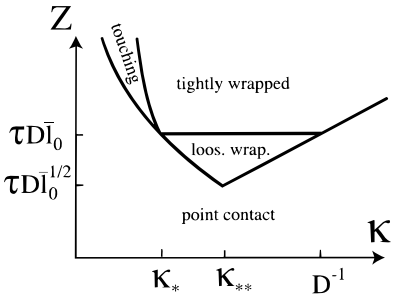

Figure 5. Complete complexation phase diagram for large bare bending rigidity $l_0 > l_B D^2\tau^2$. In contrast to Figure 4 the touching phase is only observed for extremely low salt concentrations, and in addition, we observe a loosely wrapped phase, where the radius of the wrapping polymer is larger than the sphere radius.

The wrapping transition is the continuation of the touching transition for $\kappa < \kappa_*$, eq 19, and indeed occurs below the touching transition. It is a simple matter to check that the radius of the loosely wrapped polymer R is always smaller than the screening length.

iii. High Salt, $\kappa_{**} < \kappa$. In this limit the analysis leading to eq 35 is valid.

The complete complexation diagram for stiff polymers with $\bar{l_0} > 1$ is displayed in Figure 5. Note that wrapping is the dominant phase and that the touching phase only exists in an exponentially small window. The wrapping transition is always strongly discontinuous for highly stiff polymers, both for the loosely wrapped and the tightly wrapped phase. In calculating the loosely wrapped phase, we assumed that the sphere is located in the middle of the polymer ring. In practice the sphere moves out of the center and touches the polymer ring, which slightly changes the adsorption energy but does not change the scaling of the wrapping transition.

IV. Adsorption−Desorption Transition and Fluctuation Effects

So far, we calculated the structure of a polyelectrolyte at a charged sphere, *assuming that the polymer is in contact with the sphere at one point*. In this section, we estimate the free energy of complexation and make predictions on whether the polymer is complexed with the sphere or detached from the sphere. As a simple criterion for the adsorption transition, we compare the adsorption energy with the thermal energy, k_BT . If the complexation energy is larger than k_BT, a sizable polymer fraction in bulk solution is adsorbed on spheres. We also estimate the importance of fluctuations and image-charge effects. As a result of these scaling considerations, we find that a considerable fraction of the wrapped phase found in the last section is unstable with respect to fluctuations and gives room to a nonwrapped phase, which, however, might still be a strong complex between the sphere and the polymer.

Within our perturbative treatment, the adsorption energy is divided into two pieces. The first part is the adsorption energy of the flat and unperturbed polymer, given by eq 7, which leads to the limiting

expressions

$$\frac{H_0}{k_B T} \sim -Z\tau l_B \ln\left(\frac{1}{D\kappa}\right) \tag{38}$$

for $\kappa \ll D^{-1}$ and

$$\frac{H_0}{k_B T} \sim -\frac{Z\tau l_B}{(D\kappa)^{3/2}} \tag{39}$$

for $\kappa \gg D^{-1}$. The second part is due to the deformation of the polymer and given by eq 9 with $\tilde{\theta}(\omega)$ determined by eq 15. The integral in eq 9 can be calculated using the same methods as in Appendix B, and assuming that the polymer is only in point contact with the sphere, the final result for the additional energy contribution reads

$$\frac{\Delta H}{k_B T} \sim -\frac{Z^2 l_B}{D} \ln^{-1}\left(\frac{1}{D\kappa}\right) \tag{40}$$

for $\kappa \ll D^{-1}$ and

$$\frac{\Delta H}{k_B T} \sim -\frac{Z^2 l_B}{D^{3/2}\kappa^{1/2}} \tag{41}$$

for $\kappa \gg D^{-1}$.

Comparing the two adsorption energies for $D \ll \kappa^{-1}$, eqs 38 and 40, we find the contribution of the flat adsorbed polymer, eq 38, to be dominant for $Z < D\tau \ln^2(1/D\kappa)$, which is above the wrapping transition, eq 29. For the relevant parameter range (as we discuss at the end of this section) the adsorption transition for $\kappa \ll D^{-1}$ therefore follows from eq 38 and reads

$$Z_{ads} \sim \frac{1}{\tau l_B \ln(D\kappa)^{-1}} \tag{42}$$

Comparing the two adsorption energies for $D \gg \kappa^{-1}$, eqs 39 and 41, we find the contribution of the flat adsorbed polymer, eq 39, to be dominant for $Z < \tau/\kappa$, which coincides with the wrapping transition, eq 33. For $\kappa \gg D^{-1}$ and in the unwrapped region the adsorption transition therefore follows from eq 39 and reads

$$Z_{ads} \sim \frac{D^{3/2}\kappa^{3/2}}{\tau l_B} \tag{43}$$

For $\kappa \gg D^{-1}$ and in the wrapped region the adsorption transition therefore follows from eq 41 and reads

$$Z_{ads} \sim \frac{D^{3/4}\kappa^{1/4}}{l_B^{1/2}} \tag{44}$$

The crossover between the two adsorption transitions eqs 43 and 44 occurs at

$$\kappa_+ \sim D^{-1}(l_B D\tau^2)^{2/5} \tag{45}$$

In the following, we always assume that $l_B D\tau^2 > 1$. In order to calculate the adsorption transition for $\kappa > \kappa_+$, we have to characterize the wrapped state in more details.

A. Adsorption of Charged Polymers on a Charged Curved Surface. In order to include the effect of fluctuations in the wrapped state, we use recent results for the adsorption of a charged semiflexible polymer on a *planar* charged surface, which explicitly consider polymer fluctuations.[16] It was found that, for the case of relatively stiff polymers, i.e., when the effective bending rigidity is larger than the screening length regardless of the salt concentration (which is equivalent to $\tau^2 l_B l_0 > 1$), the polymers lie flat on the substrate and form a 2D phase. A simple description of the *charge reversal* phenomenon, which is ubiquitous for polyelectrolyte adsorption and which plays an important role in various problems such as colloidal stabilization, colloidal flocculation, or charged-multilayer formation, is obtained by calculating the charge density of adsorbed phases and comparing it with the substrate charge density. Although the simple model described in ref 16 only applies to the adsorption of charged polymers on flat charged walls, e.g., DNA adsorbing on charged membranes or other charged planar substrates, it can be easily applied to the present case by identifying the charge density of the flat substrate, denoted as σ, with the sphere surface charge density, $\sigma = Z/(4\pi D^2)$. Curvature effects play only a minor role for sphere radii larger than the screening length, and the energy needed to bend the polymers on the sphere surface is included in the adsorption energy and in essence leads to the wrapping thresholds discussed in section III.B.

As shown in ref 16, the adsorbed phase of a charged polymer on an oppositely charged wall is characterized by the attractive energy between the wall and the polymer, which tends to adsorb as much polymer to the wall as possible, and the repulsion between neighboring adsorbed polymer strands (here we assume that the polymer is very long or that there is an excess of polymers in the solution). It turns out that image-charge effects, which arise if the dielectric constant of the sphere is much smaller than the one of water, are dominant for relatively stiff polymers and lead in conjunction with chain fluctuations to a desorption transition at a surface charge density $\sigma \sim \tau\kappa$.[16] For the present case this means that we expect a desorption transition for a sphere charge of

$$Z_{ads} \sim D^2\tau\kappa \tag{46}$$

If the sphere charge is larger than Z_{ads}, a lamellar phase is predicted,[16] which is an ordered array of locally parallel strands with an average lamellar spacing B_{lam}. The lamellar phase can be stabilized either by steric or electrostatic repulsion between neighboring polymer strands, with a crossover between these two phases. For the adsorption on a sphere there are subtle curvature effects, leading to topological defects (note that it is impossible to pack a stripe pattern on a spherical surface without any defects), but these effects do not affect the adsorption boundaries on a scaling level. For the present case of adsorption on a sphere the most relevant phase is the electrostatically stabilized lamellar phase, with a lamellar spacing[16]

$$B_{lam} \sim \kappa^{-1}\left[\ln\left(\frac{D^2\tau\kappa}{Z}\right) + 1\right] \tag{47}$$

and an adsorption free energy (integrated over a sphere

of surface area $4\pi D^2$)

$$F_{\mathrm{lam}} \sim -l_{\mathrm{B}} Z\tau\left[\ln\left(\frac{D^2\tau\kappa}{Z}\right)+1\right] \tag{48}$$

As one can see from eq 47, the distance between polymers is larger than the screening length for $Z < Z_{\mathrm{rev}}$ with

$$Z_{\mathrm{rev}} \sim \tau D^2\kappa \tag{49}$$

which has the same scaling as the image-charge induced desorption transition eq 46. In fact, on the basis of our results in ref 16, we expect that $Z_{\mathrm{rev}} > Z_{\mathrm{ads}}$ by a logarithmic factor. For $Z < Z_{\mathrm{rev}}$ the charge of the sphere is in fact reversed: the total charge of adsorbed polymer is $Q_{\mathrm{ads}} \sim D^2\tau/B_{\mathrm{lam}}$, and with eq 47 we obtain

$$Q_{\mathrm{ads}} \sim \frac{Z_{\mathrm{rev}}}{\ln(Z_{\mathrm{rev}}/Z)+1} \tag{50}$$

As one can easily see, $Q_{\mathrm{ads}} > Z$ for $Z < Z_{\mathrm{rev}}$. In the case $Z < Z_{\mathrm{rev}}$ the adsorption energy is also always larger than thermal energy; once the wrapped state can form via the instability mechanism discussed in section III.B, it is also thermodynamically stable in the sense that the total adsorption free energy is many times $k_{\mathrm{B}}T$. For $Z > Z_{\mathrm{rev}}$ the distance between adsorbed polymers is smaller than the screening length. The results obtained in ref 16 show that in this case the adsorbed phase can be represented by a smeared-out charge distribution, and consequently, the adsorbed polymer phase exactly compensates the sphere charge (up to numerical prefactors of the order of unity). The typical distance between polymer strands in the compensated phase (for $Z > Z_{\mathrm{rev}}$) is

$$B_{\mathrm{comp}} \sim \frac{\tau D^2}{Z} \tag{51}$$

and the adsorption free energy (integrated over a sphere of surface area $4\pi D^2$) is

$$F_{\mathrm{comp}} \sim -\frac{l_{\mathrm{B}} Z^2}{D^2\kappa} \tag{52}$$

The adsorption free energies and the polymer separations of the lamellar and the compensated phases match at the charge reversal transition Z_{rev}. The scaling description is the same whether this compensated phase is still lamellar (with B_{comp} denoting the lamellar spacing) or whether it is disordered, with many chain crossings (and B_{comp} denoting the typical distance between chain crossings). Another important point is the number of turns the wrapped polymer takes around the sphere in the lamellar phase. If the preferred lamellar spacing B_{lam} is larger than the sphere radius D, the chain does not multiply wrap. Adopting $B_{\mathrm{lam}} = D$ as the threshold, we obtain with eq 47

$$Z_{\mathrm{mul}} \sim Z_{\mathrm{rev}} \mathrm{e}^{1-D\kappa} \tag{53}$$

For $Z < Z_{\mathrm{mul}}$ the polymer only wraps once (or partially) around the sphere; for $Z > Z_{\mathrm{mul}}$ the chain wraps more than once around the sphere. The transition eq 53 is shown as a dashed line in Figure 6 for the case of small bare bending rigidity, $\bar{l}_0 < 1$, together with the wrapping transition and the desorption/adsorption transitions, which are shown as solid lines. The image-charge-induced desorption transition, eq 46, hits the wrapping transition, eq 29, at an inverse screening length of $\kappa_{++} \sim D^{-1}$. In drawing Figure 6 we assume that $\kappa_{++} > D^{-1}$ by a numerical factor. We note that the charge-reversed lamellar phase disappears completely if one has $\kappa_{++} < D^{-1}$.

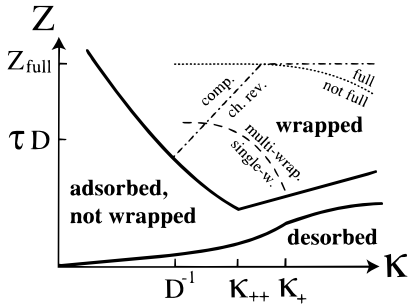

Figure 6. Phase diagram for small bare bending rigidity $l_0 < l_{\mathrm{B}}D^2\tau^2$, showing also the transition between desorbed and adsorbed phases. The adsorption transition is located by comparing the complexation energy with $k_{\mathrm{B}}T$. In addition, the wrapped phase is divided by the dashed−dotted line into a charge-reversed and a charge-compensated regime. For high salt concentration and not too high sphere charge, the sphere/polymer complex is highly charge-reversed. We also show the transition between the regime where the polymer wraps in a single loop and multiple loops around the sphere (dashed line) and the border where the adsorption layer starts to become closely packed (dotted line).

In the wrapped regime, one encounters a succession of transitions between a phase where the polymer wraps once, twice, etc., around the sphere as the sphere charge is increased. This succession of wrapping transitions stops when the sphere is covered with polymer or when it is full. In Figure 6 we show as a dotted line the boundary where the distance between neighboring polymer strands on the sphere equals the polymer diameter (which is denoted by D_{p}), which is the threshold at which the sphere surface becomes basically closely packed with adsorbed polymer. In the compensated phase this transition is obtained by comparing the polymer thickness D_{p} with the spacing in the compensated phase, eq 51, leading to the characteristic sphere charge

$$Z_{\mathrm{full}} \sim \tau D^2/D_{\mathrm{p}} \tag{54}$$

Within the lamellar phase this filling transition is obtained by comparing D_{p} with the polymer spacing in the lamellar phase, eq 47, leading to a transition at

$$Z \sim Z_{\mathrm{full}} D_{\mathrm{p}}\kappa \exp(1 - D_{\mathrm{p}}\kappa) \tag{55}$$

We do not extend the filling transition to very small salt concentrations, because the scaling arguments used in ref 16 are not applicable for $\kappa < D^{-1}$.

The wrapped phase is further subdivided into a charge-compensated regime and a charge-reversed regime, separated by a dashed−dotted line. If the surface phase is not filled with polymers, i.e., below the filling transition given by eqs 54 and 55 denoted in Figure 6 by a dotted line, the charge reversal transition is correctly given by eq 49. In the filled phase, the charge of the sphere is compensated for $Z > Z_{\mathrm{full}}$.

In the full charge-compensated phase a single adsorbed polymer layer is not sufficient to neutralize the

sphere charge. Thus, a second layer typically adsorbs and leads to a more or less complete compensation of the sphere charge. This requires that the complex formed by the sphere and the first adsorbed layer has a charge larger than the wrapping threshold. In the full charge-reversed phase, which corresponds to the narrow region between the dotted curve and the horizontal straight line in Figure 6, the complex has an effective charge of the opposite sign compared to that of the bare sphere; the first layer overcompensates the charge of the sphere, and a second layer does not adsorb.

In order not to cluster the phase diagram, we omitted the touching transition in Figure 6, which can be seen in Figure 4 and which lies completely inside the adsorbed phase. At the desorbed/adsorbed transition for low screening, $\kappa < \kappa_+$, the polymer is in a nontouching configuration and only has a point contact with the sphere. For the choice of parameters in Figure 6 we obtain always a region of an adsorbed−nonwrapped phase between the wrapped and the desorbed region. We note that for a different choice of parameters the transition between the desorbed phase and the wrapped phase can also coincide with the wrapping transition.

V. Summary

In this paper, we perturbatively calculated the shape of a semiflexible charged polymer which is in contact with an oppositely charged sphere. We found, as a function of the polymer line charge density τ, bending rigidity l_0, sphere charge Z, sphere radius D, and screening length κ^{-1}, the following different phases: For small sphere charge, the polymer shape is perturbed by the presence of the sphere but only contacts the sphere at one point. Above the touching transition, the polymer touches the sphere over a finite length, and above the wrapping transition, it completely wraps the sphere. For large salt concentration and/or large bending rigidity, the touching and wrapping transitions coincide and the wrapping is strongly discontinuous. For screening lengths smaller than the sphere radius and not too high sphere charge the wrapped phase reverses the charge of the complex. We also locate the transition where the polymer starts to wrap more than once around the sphere.

Our results can qualitatively explain two different features of nucleosomal particles. The genetic material of all eukaryotes exists in repetitive structures whose basic elements are the so-called nucleosomal core particles. They consist of 146 base pairs of negatively charged DNA (of approximate length 50 nm) wrapped around a positively charged protein core of a diameter of roughly 8 nm (the histone octamer). In the nucleus, these nucleosomal particles form, together with other chromosomal proteins, an immensely intricate complex called chromatin, the precise structure of which is not yet fully understood. The long DNA string can be broken into isolated nucleosomal particles by DNase, with which a variety of different experiments have been performed over the last years. We comment on two findings:

(i) In one type of experiment, nucleosomal particles are exposed to a salt solution of varying ionic strength.[9] It is found that a stable histone/DNA complex is only formed for salt concentrations around the physiological concentration of 0.1 M. At lower salt concentrations, at roughly 10 mM, an expanded complex is found, where the DNA is partially or completely unwrapped from the histone but seems to be still associated with the core protein. At higher salt concentrations, at roughly 1 M, free DNA is in equilibrium with free histone particles. The bare bending rigidity of DNA is about 30 nm, and at a salt concentration of about 0.1 M the effective bending rigidity is increased by 20 nm to roughly 50 nm.[23] At physiological salt concentrations the bare bending rigidity thus roughly equals the electrostatic contribution to the persistence length. The screening length for a 0.1 M monovalent salt solution is about 1 nm. (Note that the asymptotic expression $l_{OSF} = l_B\tau^2/4\kappa^2$ predicts $l_{OSF} \approx 7$ nm, where we used $l_B = 0.8$ nm and $\tau = 5.9$ nm^{-1}, which gives the right magnitude of the electrostatic contribution to the persistence length.) The histone octamers have an outer diameter of about 8 nm and are thus larger than the screening length. Since $l_0 < l_B D^2\tau^2$, the DNA/histone complex is described by Figures 4 and 6. In agreement with the experimental results, we find, starting from the wrapped situation, a transition to an unwrapped state both by lowering and by increasing the salt concentration. At the salt concentrations 10 mM and 1 M, the wrapping transitions for low and high salt concentrations, eqs 33 and 35, give a critical histone charge of roughly 20 elementary charges. This charge is much smaller than the total number of basic amino acids in the histone, which is roughly 200, but it is not clear whether all basic amino acids are dissociated at such high salt concentrations. Given the rough scaling nature of our calculation for the wrapping transition, we have to consider the agreement satisfactory. In agreement with experimental[8] and theoretical[25] results, the wrapped state occurs at $Z < \tau D$ and thus at a histone charge which does not neutralize the DNA charge completely. The DNA/histone complex is charge reversed (taking the charge of the histone as the reference state).

(ii) The unwrapping transition can also be induced by raising the temperature. The interesting finding in such experiments is that the unwrapping occurs in two stages, first wrapping up one loop and then, at a higher temperature, the second loop.[7,8] We tentatively identify the first transition with our transition between the single-wrapped and the multiply wrapped region, eq 53. Since the screening length increases as the temperature increases, we see that one goes from the multiply wrapped phase to the singly wrapped phase as temperature increases. This roughly agrees with the fact that at this intermediate transition about 50 base pairs are lost from the complex, and the remaining 95 base pairs wrap the histone just once. As can be seen in Figure 6 (noting that increasing the temperature corresponds to decreasing κ and thus going to the left in the phase diagram), upon further increasing the temperature, one goes from the singly-wrapped phase into the nonwrapped phase.

Besides the ability of histone proteins to induce tightly bound complexes, protein-induced DNA bending is common for eukaryotic transcription factors.[6] It is known that many DNA binding proteins present cationic surfaces to the DNA. A second possibility to produce DNA bends is to turn off phosphate charges on one side of the DNA.[6] Our analytical results prove that the two arms extending from the adsorption locus are uncorrelated as soon as the size of the binding protein exceeds the screening length and is mostly determined by the length over which the DNA is bound to the protein.

The qualitative results obtained in this paper have been checked by direct numerical minimization of eq 1 including the hard-core constraint of the sphere.[22] In the future, we would like to extend our calculations to three dimensions and include the effects of many adsorbed spheres.

Acknowledgment. We acknowledge useful discussions with W. Gelbart, G. Manning, and F. Pincus. This research was supported by the Deutsche Forschungs Gemeinschaft through the Schwerpunkt "Polyelektrolyte".

Appendix A: Fourier Transform of *g*(*s*)

Using the definition of the function $g(s)$, eq 6, the Fourier transform $\tilde{g}(\omega)$ is given by

$$\tilde{g}(\omega) = -2\tau ZD \int_0^\infty \mathrm{d}s \cos[s\omega] \int_s^\infty \mathrm{d}s' \times \frac{v'_{sp}(\sqrt{D^2+s'^2})(s'-s)}{\sqrt{D^2+s'^2}} \quad \text{(A1)}$$

which yields after some manipulations

$$\tilde{g}(\omega) = -\frac{2\tau ZD}{\omega^2} \int_0^\infty \mathrm{d}s \frac{v'_{sp}(\sqrt{D^2+s^2})}{\sqrt{D^2+s^2}}(1-\cos[s\omega]) \quad \text{(A2)}$$

1. Behavior for Small *ω*. After a partial integration, eq A2 takes the form

$$\tilde{g}(\omega) = 2\tau ZD \int_0^\infty \mathrm{d}s\, v_{sp}(\sqrt{D^2+s^2}) \times \frac{s\omega \sin[s\omega] - 1 + \cos[s\omega]}{s^2\omega^2} \quad \text{(A3)}$$

Using now the specific form of v_{sp}, eq 3, and the definitions $d = D\kappa$ and $\bar{\omega} = \omega/\kappa$, the integral is

$$\tilde{g}(\bar{\omega}) = \frac{2\tau ZDl_B \mathrm{e}^d}{1+d} \int_0^\infty \mathrm{d}x \times \frac{\mathrm{e}^{-\sqrt{d^2+x^2}}}{\sqrt{d^2+x^2}} \frac{x\bar{\omega}\sin[x\bar{\omega}] - 1 + \cos[x\bar{\omega}]}{x^2\bar{\omega}^2} \quad \text{(A4)}$$

The momentum-dependent part can be expanded for small momenta,

$$\frac{x\bar{\omega}\sin[x\bar{\omega}] - 1 + \cos[x\bar{\omega}]}{x^2\bar{\omega}^2} = \frac{1}{2} - \frac{(x\bar{\omega})^2}{8} + \frac{(x\bar{\omega})^4}{144} + \ldots \quad \text{(A5)}$$

and each term can be integrated yielding

$$\int_0^\infty \mathrm{d}x \frac{\mathrm{e}^{-\sqrt{d^2+x^2}}}{\sqrt{d^2+x^2}} x^{2n} = (2n-1)!!\, d^n K_n[d] \quad \text{(A6)}$$

The resulting first terms in the small-ω expansion are

$$\tilde{g}(\bar{\omega}) = \frac{2\tau ZDl_B \mathrm{e}^d}{1+d}\left(\frac{1}{2}K_0[d] - \frac{\bar{\omega}^2 d}{8}K_1[d] + \frac{\bar{\omega}^4 d^2}{48}K_2[d] + \ldots\right) \quad \text{(A7)}$$

The asymptotic expressions are

$$\tilde{g}(\bar{\omega}) \simeq \tau ZDl_B\left(-\ln(d/2) - \frac{\bar{\omega}^2}{4} + \frac{\bar{\omega}^4}{12} + \ldots\right) \quad \text{(A8)}$$

for $d \ll 1$ and

$$\tilde{g}(\bar{\omega}) \simeq \sqrt{\frac{\pi}{2}}\frac{\tau ZDl_B}{d^{3/2}}\left(1 - \frac{\bar{\omega}^2 d}{4} + \frac{\bar{\omega}^4 d^2}{24} + \ldots\right) \quad \text{(A9)}$$

for $d \gg 1$.

2. Behavior for Small *d*. Now we rewrite eq A2 using the integration variable $t = s\kappa/d$ and $\bar{\omega} = \omega/\kappa$, inserting the expression for v_{sp}, and obtain

$$\tilde{g}(\bar{\omega}) = \frac{2\tau ZDl_B}{(\bar{\omega}d)^2} \int_0^\infty \mathrm{d}t \left[\frac{\mathrm{e}^{-d\sqrt{1+t^2}}}{(1+t^2)^{3/2}} + d\frac{\mathrm{e}^{-d\sqrt{1+t^2}}}{1+t^2}\right] \times (1-\cos[t(\bar{\omega}d)]) \quad \text{(A10)}$$

The integrand can now be expanded with respect to d. The leading result is

$$\tilde{g}(\bar{\omega}) \simeq \frac{2\tau ZDl_B}{(\bar{\omega}d)^2} \int_0^\infty \mathrm{d}t \frac{1-\cos[t(\bar{\omega}d)]}{(1+t^2)^{3/2}} = \frac{2\tau ZDl_B}{(\bar{\omega}d)^2}(1 - \bar{\omega}dK_1[\bar{\omega}d]) \quad \text{(A11)}$$

The asymptotic limits of this expression are

$$\tilde{g}(\bar{\omega}) \simeq \frac{2\tau ZDl_B}{(\bar{\omega}d)^2}(1 - \sqrt{\pi\bar{\omega}d/2}\,\mathrm{e}^{-\bar{\omega}d}) \quad \text{(A12)}$$

for $\bar{\omega}d \gg 1$ and

$$\tilde{g}(\bar{\omega}) \simeq -\tau ZDl_B \ln(\bar{\omega}d/2) \quad \text{(A13)}$$

for $\bar{\omega}d \ll 1$.

3. Behavior for Large *d*. Now we rewrite eq A2 using the integration variable $x = s\kappa$ and $\bar{\omega} = \omega/\kappa$, inserting the expression for v_{sp} in the limit $d \gg 1$, and obtain

$$\tilde{g}(\bar{\omega}) = \frac{\tau ZDl_B}{\bar{\omega}^2 d} \int_{-\infty}^\infty \mathrm{d}x \left[\frac{\mathrm{e}^{-\sqrt{d^2+x^2}}}{d^2+x^2} + \frac{\mathrm{e}^{-\sqrt{d^2+x^2}}}{(d^2+x^2)^{3/2}}\right] \times (1-\cos[\bar{\omega}x]) \quad \text{(A14)}$$

Using the integration variable $z = ((1+x^2/d^2)^{1/2} - 1)^{1/2}$, the integral becomes

$$\tilde{g}(\bar{\omega}) = \frac{2\tau ZDl_B}{\bar{\omega}^2 d^2} \int_{-\infty}^\infty \mathrm{d}z \left[\frac{\mathrm{e}^{-dz^2}}{(1+z^2)(2+z^2)^{1/2}} + \frac{1}{d}\frac{\mathrm{e}^{-dz^2}}{d(1+z^2)^2(2+z^2)^{1/2}}\right](1-\cos[\bar{\omega}dz(2+z^2)^{1/2}]) \quad \text{(A15)}$$

The second term is of higher order in an expansion in

powers of d^{-1} and can be neglected. The remaining integral consists of two parts, $\tilde{g}(\bar{\omega}) = (\tau Z D l_B/\bar{\omega}^2 d^2)(I_1 + I_2)$ with

$$I_1 = 2\int_{-\infty}^{\infty} dz\, \frac{e^{-dz^2}}{(1+z^2)(2+z^2)^{1/2}} \tag{A16}$$

which can be solved by a expansion in powers of z and yields

$$I_1 = \sqrt{2}\int_{-\infty}^{\infty} dz\, e^{-dz^2}\left(1 - \frac{5}{4}z^2 + ...\right) = \sqrt{\frac{2\pi}{d}}\left(1 - \frac{5}{8d} + ...\right) \tag{A17}$$

The second integral I_2 can be evaluated using saddle-point methods. Using the representation $2\cos[x] = e^{ix} + e^{-ix}$, we define

$$I_2 = -2\int_{-\infty}^{\infty} dz\, \frac{e^{-dz^2 + i\bar{\omega}dz(2+z^2)^{1/2}}}{(1+z^2)(2+z^2)^{1/2}} \equiv -2\int_{-\infty}^{\infty} dz\, e^{-f(z)} \tag{A18}$$

with

$$f(z) = dz^2 + \ln(1+z^2) + \frac{1}{2}\ln(2+z^2) - i\bar{\omega}dz(2+z^2)^{1/2} \tag{A19}$$

The saddle point z^* is determined by the equation $f'(z^*) = 0$, and the integral I_2 is given by

$$I_2 \simeq -2e^{-f(z^*)}\int_{-\infty}^{\infty} dz\, e^{-f''(z^*)z^2/2} = -2\sqrt{\frac{2\pi}{f''(z^*)}}e^{-f(z^*)} \tag{A20}$$

We find three different saddle point for different values of $\bar{\omega}$:

(i) For $\bar{\omega} \ll 1$, we obtain $z^* \simeq i\bar{\omega}/\sqrt{2}$ and thus $f(z^*) \simeq d\bar{\omega}^2/2 + \ln(\sqrt{2})$ and $f''(z^*) \simeq 2d$. The result for I_2 is

$$I_2 \simeq -\sqrt{\frac{2\pi}{d}}e^{-d\bar{\omega}^2/2}$$

(ii) For $1 \ll \bar{\omega} \ll d$, we obtain $z^* \simeq i(1 - (\bar{\omega}d)^{-1/2}/2)$ and thus $f(z^*) \simeq \bar{\omega}d - \ln(\bar{\omega})$ and $f''(z^*) \simeq 4\bar{\omega}d$. The result for I_2 is

$$I_2 \simeq -\frac{\sqrt{2\pi\bar{\omega}}}{d}e^{-d\bar{\omega}}$$

(iii) For $1 \ll d \ll \bar{\omega}d$, we obtain $z^* \simeq i(1 - \bar{\omega}^{-1}/2)$ and thus $f(z^*) \simeq \bar{\omega}d - (1/2)\ln(\bar{\omega}d)$ and $f''(z^*) \simeq 8\bar{\omega}d$. The result for I_2 is

$$I_2 \simeq -\sqrt{\pi}e^{-d\bar{\omega}}$$

Adding up the two integrals I_1 and I_2 we obtain for $\bar{\omega} \ll 1$

$$\tilde{g}(\bar{\omega}) \simeq \frac{\sqrt{2\pi}\tau Z D l_B}{\bar{\omega}^2 d^{5/2}}(1 - e^{-d\bar{\omega}^2/2}) \tag{A21}$$

For very small $\bar{\omega}$, i.e. $\bar{\omega} \ll d^{-1/2} \ll 1$, we can expand the exponential and obtain as the leading term

$$\tilde{g}(\bar{\omega}) \simeq \frac{\sqrt{\pi}\tau Z D l_B}{2\ d^{3/2}} \tag{A22}$$

which agrees exactly with our result obtained using the systematic small-$\bar{\omega}$ expansion, eq A9. For larger values of $\bar{\omega}$, i.e. $\bar{\omega} \gg d^{-1/2}$, we can neglect the exponential corrections from I_2 and obtain as the leading term

$$\tilde{g}(\bar{\omega}) \simeq \frac{\sqrt{2\pi}\tau Z D l_B}{\bar{\omega}^2 d^{5/2}} \tag{A23}$$

4. Summary. Keeping only the leading terms, we obtain for $d \ll 1$

$$\tilde{g}(\bar{\omega}) \simeq Z D \tau l_B \times \begin{cases} -\ln(d/2) & \text{for } \bar{\omega} \ll 1 \ll d^{-1} \\ -\ln(\bar{\omega}d/2) & \text{for } 1 \ll \bar{\omega} \ll d^{-1} \\ 2\bar{\omega}^{-2}d^{-2} & \text{for } 1 \ll d^{-1} \ll \bar{\omega} \end{cases} \tag{A24}$$

and for $d \gg 1$

$$\tilde{g}(\bar{\omega}) \simeq \sqrt{\frac{\pi}{2}}\frac{Z D \tau l_B}{d^{3/2}} \times \begin{cases} 1 & \text{for } \bar{\omega} \ll d^{-1/2} \ll 1 \\ 2\bar{\omega}^{-2}d^{-1} & \text{for } d^{-1/2} \ll \bar{\omega} \end{cases} \tag{A25}$$

Appendix B: Calculation of the Curvature at the Origin

Here we calculate the curvature at the origin using eq 12. It is convenient to rescale all length scales by the screening length κ^{-1}; we thus use the rescaled momentum $\bar{\omega} = \omega/\kappa$ and the rescaled sphere radius $d = D\kappa$. The rescaled version of eq 12 reads

$$\dot{\theta}_0 = \kappa\int \frac{d\bar{\omega}}{2\pi}\frac{\tilde{g}(\bar{\omega}) + h}{\tilde{K}(\bar{\omega}) + l_0 + \bar{m}\bar{\omega}^2} \tag{B1}$$

Since we are interested in the asymptotic behavior, we only need the leading terms of $\tilde{g}(\bar{\omega})$, given in eqs A24 and A25, and $\tilde{K}(\bar{\omega})$, which follows from eq 11 in rescaled units as

$$\tilde{K}(\bar{\omega}) \simeq \begin{cases} l_{OSF} & \text{for } \bar{\omega} \ll 1 \\ 4l_{OSF}\bar{\omega}^{-2}\ln(\bar{\omega}) & \text{for } \bar{\omega} \gg 1 \end{cases} \tag{B2}$$

1. Integrals for $l_0 = 0$ and $D \ll \kappa^{-1}$. Assuming that h and $\bar{m}$ are chosen such that they dominate the integrand for rescaled momenta $\bar{\omega} > \bar{\omega}_* \gg d^{-1}$, according to our discussion in section III.B this means that the polymer touches the sphere over a length smaller than the sphere radius D. We can separate the integral in eq B1 in four parts,

$$\dot{\theta}_0 \sim \frac{Z d \tau l_B}{l_{OSF}}(I_1 + I_2 + I_3 + I_4) \tag{B3}$$

with

$$I_1 = \int_0^1 \mathrm{d}\bar{\omega}\, \ln(d^{-1}) \sim \ln\, d^{-1} \tag{B4}$$

$$I_2 = \int_1^{d^{-1}} \mathrm{d}\bar{\omega}\, \frac{\bar{\omega}^2(1 - \ln(\bar{\omega}d))}{\ln\, \bar{\omega}} \sim \frac{d^{-3}}{\ln\, d^{-1}} \tag{B5}$$

$$I_3 = \frac{1}{d^2} \int_{d^{-1}}^{\bar{\omega}_*} \mathrm{d}\bar{\omega}\, \frac{1}{\ln\, \bar{\omega}} \sim \frac{\bar{\omega}_*}{d^2 \ln\, \bar{\omega}_*} \tag{B6}$$

$$I_4 = \frac{l_{\mathrm{OSF}} h}{ZD\tau l_{\mathrm{B}} \bar{m}} \int_{\bar{\omega}_*}^{\infty} \mathrm{d}\bar{\omega}\, \frac{1}{\bar{\omega}^2} \sim \frac{l_{\mathrm{OSF}} h}{ZD\tau l_{\mathrm{B}} \bar{m} \bar{\omega}_*} \tag{B7}$$

The equations determining h and $\bar{m}$ in terms of $\bar{\omega}_*$ are $\tilde{g}(\bar{\omega}_*) = h$ and $\tilde{K}(\bar{\omega}_*) = \bar{m}\bar{\omega}_*^2$. Using the condition $\bar{\omega}_* \gg d^{-1}$ and the eqs A24 and B2 we thus obtain

$$h \sim \frac{ZD\tau l_{\mathrm{B}}}{\bar{\omega}_*^{\,2} d^2}$$

$$\bar{m} \sim \frac{l_{\mathrm{OSF}} \ln\, \bar{\omega}_*}{\bar{\omega}_*^{\,4}}$$

As a result, we see that $I_4 \sim I_3 \gg I_2 \gg I_1$. The final result for the curvature at the origin is

$$\dot{\theta}_0 \sim \frac{Z\tau l_{\mathrm{B}}}{d l_{\mathrm{OSF}}} \frac{\bar{\omega}_*}{\ln\, \bar{\omega}_*} \sim \frac{Z}{D\tau} \frac{\omega_*}{\ln(\omega_* \kappa^{-1})} \tag{B8}$$

2. Integrals for $l_0 = 0$ and $D \gg \kappa^{-1}$. With the same definition as in eq B3 and assuming that $\bar{\omega}_* \gg 1$ we have

$$I_1 = d^{-3/2} \int_0^{d^{-1/2}} \mathrm{d}\bar{\omega} \sim d^{-2} \tag{B9}$$

$$I_2 = d^{-5/2} \int_{d^{-1/2}}^1 \mathrm{d}\bar{\omega}\, \frac{1}{\bar{\omega}^2} \sim d^{-2} \tag{B10}$$

$$I_3 = d^{-5/2} \int_1^{\bar{\omega}_*} \mathrm{d}\bar{\omega}\, \frac{1}{\ln\, \bar{\omega}} \sim \frac{\bar{\omega}_*}{d^{5/2} \ln\, \bar{\omega}_*} \tag{B11}$$

$$I_4 = \frac{l_{\mathrm{OSF}} h}{ZD\tau l_{\mathrm{B}} \bar{m}} \int_{\bar{\omega}_*}^{\infty} \mathrm{d}\bar{\omega}\, \frac{1}{\bar{\omega}^2} \sim \frac{l_{\mathrm{OSF}} h}{ZD\tau l_{\mathrm{B}} \bar{m} \bar{\omega}_*} \tag{B12}$$

The equations determining h and $\bar{m}$ are $\tilde{g}(\bar{\omega}_*) = h$ and $\tilde{K}(\bar{\omega}_*) = \bar{m}\bar{\omega}_*^2$, which for $D \gg \kappa^{-1}$ and $\bar{\omega}_* \gg 1$ yield

$$h \sim \frac{ZD\tau l_{\mathrm{B}}}{\bar{\omega}_*^{\,2} d^{5/2}}$$

$$\bar{m} \sim \frac{l_{\mathrm{OSF}} \ln\, \bar{\omega}_*}{\bar{\omega}_*^{\,4}}$$

As a result, we see that $I_4 \sim I_3$. The final result for the curvature at the origin is

$$\dot{\theta}_0 \sim \frac{Z\tau l_{\mathrm{B}}}{d l_{\mathrm{OSF}}}\left(1 + \frac{\bar{\omega}^*}{d^{1/2} \ln\, \bar{\omega}^*}\right) \sim \frac{Z\kappa}{\tau D}\left(1 + \frac{\omega_*}{D^{1/2}\kappa^{3/2} \ln(\omega_* \kappa^{-1})}\right) \tag{B13}$$

3. Integrals for $l_0 > 0$ and $D \ll \kappa^{-1}$. In the case of a finite bare bending rigidity, $l_0 > 0$, the curvature at the origin stays always finite. We set the constants h and $\bar{m}$ appearing in eq B1 to zero and discuss at the end the result if these constants are nonzero. For $l_0 > l_{\mathrm{OSF}}$, the bare bending rigidity l_0 is for all momenta more relevant than the electrostatic persistence length l_{OSF}; this case will be treated in section B.3.c. For $l_0 < l_{\mathrm{OSF}}$, there is a crossover scale $\bar{\omega}_0$ at which the bare bending rigidity becomes relevant, determined by the equation $\tilde{K}(\bar{\omega}_0) \simeq l_0$. Using the asymptotic expansion of $\tilde{K}$, eq B2, this equation is explicitly given by

$$\frac{l_{\mathrm{OSF}} \ln\, \bar{\omega}_0}{\bar{\omega}_0^{\,2}} \sim l_0 \tag{B14}$$

and has the asymptotic solution

$$\bar{\omega}_0^{\,2} \sim \frac{l_{\mathrm{OSF}}}{l_0} \ln\left(\frac{l_{\mathrm{OSF}}}{l_0}\right) \tag{B15}$$

Depending on the magnitude of this scale we obtain the following results.

a. Low Salt Concentration, $\bar{\omega}_0 \gg d^{-1} \gg 1$. The condition $\bar{\omega}_0 \gg d^{-1}$ can with eq B14 be transformed into $l_0/l_{\mathrm{OSF}} \ll d^2 \ln(d^{-1}) \ll 1$. It is convenient to use the rescaled bare bending rigidity $\bar{l}_0 \equiv l_0/l_{\mathrm{B}} D^2 \tau^2$. The condition $\bar{\omega}_0 \gg d^{-1} \gg 1$ is satisfied if the salt concentration is low, for $\kappa \ll \kappa_* < D^{-1}$, where $\kappa_* \equiv D^{-1} \mathrm{e}^{-\bar{l}_0}$. The integrals to be solved are the same as in Appendix B.1. Using the definition eq B3 we obtain I_1 and I_2 as in eqs B4 and B5 and

$$I_3 = \frac{1}{d^2} \int_{d^{-1}}^{\bar{\omega}_0} \mathrm{d}\bar{\omega}\, \frac{1}{\ln\, \bar{\omega}} \sim \frac{\bar{\omega}_0}{d^2 \ln\, \bar{\omega}_0} \tag{B16}$$

$$I_4 = \frac{l_{\mathrm{OSF}}}{l_0 d^2} \int_{\bar{\omega}_0}^{\infty} \mathrm{d}\bar{\omega}\, \frac{1}{\bar{\omega}^2} \sim \frac{l_{\mathrm{OSF}}}{l_0 d^2 \bar{\omega}_0} \tag{B17}$$

With the definition of the crossover scale, eq B14, we see that $I_3 \sim I_4$. Since $\bar{\omega}_0 \gg d^{-1} \gg 1$, we have $I_3 \gg I_2 \gg I_1$, so that the final result for the curvature at the origin reads

$$\dot{\theta}_0 \sim \frac{Z\tau l_{\mathrm{B}}}{\mathrm{d} l_{\mathrm{OSF}}} \frac{\bar{\omega}_0}{\ln\, \bar{\omega}_0} \sim \frac{Z}{D^2 \tau \bar{l}_0^{\,1/2}} \ln^{-1/2}\left(\frac{1}{\bar{l}_0 D^2 \kappa^2}\right) \tag{B18}$$

It is important to note that the dependence of this result on the crossover scale $\bar{\omega}_0$ is identical to the dependence of the analogous result eq B8 on the parameter $\bar{\omega}_*$ (where $\bar{\omega}_*$ is a measure of the extent over which the polymer touches the sphere). It follows that if the bare persistence length is not sufficiently strong to keep the curvature at the origin smaller than the sphere curvature, we can switch from eq B18 to the result obtained with the boundary terms used to control $\dot{\theta}_0$, eq B8, obtained without a bare persistence length. The bare persistence length becomes irrelevant at the point where the polymer starts touching the sphere over a finite length.

b. Intermediate Salt Concentration, $d^{-1} \gg \bar{\omega}_0 \gg 1$. The conditions defining this regime can with eq B14 be transformed into $d^2 \ln(d^{-1}) \ll l_0/l_{\mathrm{OSF}} \ll 1$. With the rescaled bare bending rigidity we can reformulate these conditions as $\kappa_* \ll \kappa \ll \kappa_{**}$ where $\kappa_{**} \equiv D^{-1} \bar{l}_0^{-1/2}$. With the same definition as in eq B3 we get I_1 as in eq B4

and

$$I_2 = \int_1^{\bar{\omega}_0} \mathrm{d}\bar{\omega}\, \frac{\bar{\omega}^2(1 - \ln(\bar{\omega}\mathrm{d}))}{\ln \bar{\omega}} \sim \frac{\bar{\omega}_0{}^3}{\ln \bar{\omega}_0}(1 - \ln(\bar{\omega}_0 d)) \quad \text{(B19)}$$

$$I_3 = \frac{l_{\mathrm{OSF}}}{l_0} \int_{\bar{\omega}_0}^{d^{-1}} \mathrm{d}\bar{\omega}\, (1 - \ln(\bar{\omega} d)) \sim \frac{l_{\mathrm{OSF}}}{l_0 d} \quad \text{(B20)}$$

$$I_4 = \frac{l_{\mathrm{OSF}}}{l_0 d^2} \int_{d^{-1}}^{\infty} \mathrm{d}\bar{\omega}\, \frac{1}{\bar{\omega}^2} \sim \frac{l_{\mathrm{OSF}}}{l_0 d} \quad \text{(B21)}$$

and again we have $I_3 \sim I_4$. With the help of eq B14 we find $I_3 \gg I_2 \gg I_1$, so that the final result for the curvature at the origin reads

$$\dot{\theta}_0 \sim \frac{Z\tau l_{\mathrm{B}}}{l_0} \sim \frac{Z}{D^2 \tau \bar{l_0}} \quad \text{(B22)}$$

c. High Salt Concentration, $l_0 \gg l_{\mathrm{OSF}}$ and $d \ll 1$. The condition $l_0 \gg l_{\mathrm{OSF}}$ is equivalent to $\kappa \gg \kappa_{**}$. We separate the integral in eq B1 in three parts,

$$\dot{\theta}_0 \sim \frac{Zd\tau l_{\mathrm{B}}}{l_0}(I_1 + I_2 + I_3) \quad \text{(B23)}$$

where I_1 is given in eq B4 and

$$I_2 = \int_1^{d^{-1}} \mathrm{d}\bar{\omega}\, (1 - \ln(\bar{\omega} d)) \sim d^{-1} \quad \text{(B24)}$$

$$I_3 = \frac{1}{d^2} \int_{d^{-1}}^{\infty} \mathrm{d}\bar{\omega}\, \frac{1}{\bar{\omega}^2} \sim d^{-1} \quad \text{(B25)}$$

Clearly, since $d \ll 1$, we have $I_3 \sim I_2 \gg I_1$ and we obtain the same result as in eq B22,

$$\dot{\theta}_0 \sim \frac{Z\tau l_{\mathrm{B}}}{l_0} \sim \frac{Z}{D^2 \tau \bar{l_0}} \quad \text{(B26)}$$

4. Integrals for $l_0 > 0$ and $D \gg \kappa^{-1}$. *a. Low and Intermediate Salt Concentration, $l_0 < l_{\mathrm{OSF}}$.* For $l_0 < l_{\mathrm{OSF}}$, corresponding to $\kappa < \kappa_{**}$, we again find a crossover scale $\bar{\omega}_0 > 1$ which separates a length-scale range dominated by the bare bending rigidity (for small length scales) from a length-scale range dominated by the electrostatic contribution to the persistence length (for large length scales). This crossover scale is determined by eq B14 with the solution eq B15. With the same definition as in eq B3 we obtain I_1 and I_2 as in eqs B9 and B10 and

$$I_3 = d^{-5/2} \int_1^{\bar{\omega}_0} \mathrm{d}\bar{\omega}\, \frac{1}{\ln \bar{\omega}} \sim \frac{\bar{\omega}_0}{d^{5/2} \ln \bar{\omega}_0} \quad \text{(B27)}$$

$$I_4 = \frac{l_{\mathrm{OSF}}}{d^{5/2} l_0} \int_{\bar{\omega}_0}^{\infty} \mathrm{d}\bar{\omega}\, \frac{1}{\bar{\omega}^2} \sim \frac{l_{\mathrm{OSF}}}{d^{5/2} l_0 \bar{\omega}_0} \quad \text{(B28)}$$

Clearly, we have $I_1 \sim I_2$. Using the scaling behavior of the crossover scale $\bar{\omega}_0$, as determined by eq B14, we see that $I_4 \sim I_3$. The final result for the curvature at the origin is, using eq B15,

$$\dot{\theta}_0 \sim \frac{Z\tau l_{\mathrm{B}}}{l_{\mathrm{OSF}} d}\left(1 + \frac{\bar{\omega}_0}{d^{1/2} \ln \bar{\omega}_0}\right) \sim \frac{Z\kappa}{\tau D}\left(1 + \left[\frac{1}{\bar{l_0} D^3 \kappa^3 \ln(1/\bar{l_0}\kappa^2 D^2)}\right]^{1/2}\right) \quad \text{(B29)}$$

We note that there is a crossover in the solution which occurs for $d \ln(l_{\mathrm{OSF}}/l_0) \sim (l_{\mathrm{OSF}}/l_0)$ or, in terms of the screening length, at $\kappa \sim \kappa_{***}$ with $\kappa_{***} \equiv D^{-1}(\bar{l_0} \ln \bar{l_0}^{-1})^{1/3}$. Also, the solution is identical to the one without bare persistence length but with constraints fixing the polymer curvature at the origin; see eq B13. Above the touching transition one can neglect the presence of a bare persistence length and switch continuously from the solution eq B29 to solution eq B13.

b. High Salt Concentration, $l_0 > l_{\mathrm{OSF}}$. For $\kappa > \kappa_{**}$, the integral in eq B1 consists of two parts,

$$\dot{\theta}_0 \sim \frac{Z\tau l_{\mathrm{B}}}{l_0 d^{1/2}}\left(\int_0^{d^{-1/2}} \mathrm{d}\bar{\omega} + \frac{1}{d}\int_{d^{-1/2}}^{\infty} \mathrm{d}\bar{\omega}\, \frac{1}{\bar{\omega}^2}\right) \sim \frac{Z\tau l_{\mathrm{B}}}{l_0 d} \sim \frac{Z}{\bar{l_0}\kappa\tau D^3} \quad \text{(B30)}$$

Appendix C: Wrapping Energy for Low Salt

Here we calculate the increase in electrostatic self-energy of a charged polymer associated to its wrapping around a central charge, as shown schematically in Figure 3. The reference state, Figure 3a, corresponds to a straight polymer at a closest distance R from the charge. In the wrapped state, Figure 3b, the portion of the polymer which is drawn as a broken line is now wrapped on a circle around the central charge with a radius R. The length of the broken line is $2\pi R$. The polymer-self-energy difference between the two configurations consists of three parts: (i) the interaction between the two solid lines; (ii) the self-interaction of the broken line; (iii) the interaction between the broken line and the solid lines.

We start with contribution i. The electrostatic interaction between the two solid lines with a distance $L = 2\pi R$ in Figure 3a is

$$w = l_{\mathrm{B}}\tau^2 \int_0^{\infty} \mathrm{d}s \int_0^{\infty} \mathrm{d}s'\, \frac{\mathrm{e}^{-\kappa(L+s+s')}}{L+s+s'} = \frac{l_{\mathrm{B}}\tau^2}{\kappa}(\mathrm{e}^{-\kappa L} - \kappa L \Gamma[0, \kappa L])$$

The self-energy difference of the interaction between the two solid lines in Figure 3a,b thus becomes in the limit $\kappa L = 2\pi R\kappa \ll 1$

$$f^{\,\mathrm{i}}_{\mathrm{rep}} \simeq -2\pi l_{\mathrm{B}}\tau^2 R \ln(\kappa R) \quad \text{(C1)}$$

where we used the behavior of the incomplete Gamma function for small arguments: $\Gamma[0, s] \simeq -\ln(s)$. The self-energy difference is repulsive; i.e., one needs to do work on the system to bring the two straight arms closer together as one goes from the configuration shown in Figure 3a to the one shown in Figure 3b. In the limit of no salt, this energy increase is infinite for infinitely long arms. If the arms are shorter than the screening length, the correct self-energy difference is obtained by replac-

ing the screening length by the lengths of the polymer arms in eq C1.

For contribution ii we need to calculate the bending energy of the broken line. Since we are interested in the limit where the bending radius is much smaller than the screening length, we can set the screening length to infinity, so that we get

$$f_{\mathrm{rep}}^{\mathrm{ii}} \simeq l_{\mathrm{B}} R\tau^2 \int_0^{2\pi} \mathrm{d}\gamma \int_\gamma^{2\pi} \mathrm{d}\gamma' \left[\frac{1}{2\sin[(\gamma'-\gamma)/2]} - \frac{1}{\gamma'-\gamma}\right]$$
$$= l_{\mathrm{B}} R\tau^2 \int_0^{2\pi} \mathrm{d}\gamma \left[\frac{1}{2\sin[\gamma/2]} - \frac{1}{\gamma}\right]$$
$$\simeq 3.44 l_{\mathrm{B}} R\tau^2 \qquad \text{(C2)}$$

In the limit of large κR this term can be neglected in comparison with the first contribution, eq C1.

For contribution iii we first evaluate the interaction between the broken line and the solid lines in Figure 3a, where all polymer sections are straight. The energy reads

$$w_{\mathrm{a}} = 2l_{\mathrm{B}}\tau^2 \int_0^L \mathrm{d}s \int_0^\infty \mathrm{d}s' \frac{\mathrm{e}^{-\kappa(s+s')}}{s+s'} = \frac{2l_{\mathrm{B}}\tau^2}{\kappa} \int_0^{L\kappa} \mathrm{d}s\, \Gamma[0, s]$$

In the limit of large screening length we only need the asymptotic behavior for small arguments of the incomplete Gamma function, $\Gamma[0, s] \simeq -\ln s$, and obtain with $L = 2\pi R$

$$w_{\mathrm{a}} \simeq -4\pi l_{\mathrm{B}}\tau^2 R \ln(\kappa R)$$

To obtain the scaling of the interaction between the broken curve and the solid lines in Figure 3b, we replace the charge distribution of the broken line by a point charge of magnitude $2\pi R\tau$ located in the center of the circle. The interaction then is

$$w_{\mathrm{b}} = 2\pi l_{\mathrm{B}}\tau^2 R \int_0^\infty \mathrm{d}s \frac{\mathrm{e}^{-\kappa\sqrt{s^2+R^2}}}{\sqrt{s^2+R^2}} = 4\pi l_{\mathrm{B}}\tau^2 R K_0[\kappa R]$$

With the asymptotic behavior of the modified Bessel function, $K_0[\kappa R] = -\ln(\kappa R)$, we obtain

$$w_{\mathrm{b}} \simeq -4\pi l_{\mathrm{B}}\tau^2 R \ln(\kappa R)$$

On the scaling level, the interaction energies between the broken and solid curves in Figure 3a,b are the same; it follows that the difference also has the same scaling, unless the leading terms in w_{a} and w_{b} cancel, which is unlikely and in any case not calculable within such simple scaling schemes. Even if the two terms cancel, this would not change our main conclusion, since in this case the contribution in eq C1 would dominate. We see that the total polymer self-energy difference between the configurations shown in Figure 3a,b scales as

$$f_{\mathrm{rep}} \sim -l_{\mathrm{B}}\tau^2 R \ln(\kappa R) \qquad \text{(C3)}$$

Since this energy is dominated by the repulsion between the two straight arm segments which are drawn closer to each other during wrapping, it follows that the scaling form of eq C3 is rather insensitive to the detailed configuration of the polymer in the vicinity of the sphere. This means that the wrapping transition for low salt concentrations which is shown in Figures 4 and 5 and which follows from eq C3 is probably quite reliable.

References and Notes

(1) Dautzenberg, H.; Jaeger, W.; Kötz, B. P. J.; Seidel, C.; Stscherbina, D. *Polyelectrolytes: Formation, characterization and application*; Hanser Publishers: Munich, Vienna, New York, 1994.
(2) Förster, S.; Schmidt, M. *Adv. Polym. Sci.* **1995**, *120*, 50.
(3) Barrat, J.-L.; Joanny, J.-F. *Adv. Chem. Phys.* **1996**, *94*, 1.
(4) Donath, E.; Sukhorukov, G. B.; Caruso, F.; Davis, S. A.; Möhwald, H. *Angew. Chem., Int. Ed. Engl.* **1998**, *16*, 37. Sukhorukov, G. B.; Donath, E.; Davis, S. A.; Lichtenfeld, H.; Caruso, F.; Popov, V. I.; Möhwald, H. *Polym. Adv. Technol.* **1998**, *9*, 759.
(5) Caruso, F.; Caruso, R. A.; Möhwald, H. *Science* **1998**, *282*, 1111. Caruso, F.; Lichtenfeld, H.; Giersig, M.; Möhwald, H. *J. Am. Chem. Soc.* **1998**, *120*, 8523. Caruso, F.; Donath, E.; Möhwald, H. *J. Phys. Chem. B* **1998**, *102*, 2011.
(6) Strauss, J. K.; Maher, L. J.. III. *Science* **1994**, *266*, 1829.
(7) Simpson, R. T. *J. Biol. Chem.* **1979**, *254*, 10123.
(8) McGhee, J. D.; Felsenfeld, G. *Nucleic Acids Res.* **1980**, *8*, 2751.
(9) Yager, T. D.; McMurray, C. T.; van Holde, K. E. *Biochemistry* **1989**, *28*, 2271.
(10) Dubin, P. L.; Rigsbee, D. R.; Gan, L.-M.; Fallon, M. A. *Macromolecules* **1988**, *21*, 2555. Dubin, P. L.; Kaplan, J. I.; Hua, J. *Langmuir* **1990**, *6*, 707. McQuigg, D. W.; Kaplan, J. I.; Dubin, P. L. *J. Phys. Chem* **1992**, *96*, 1973.
(11) Wallin, T.; Linse, P. *Langmuir* **1996**, *12*, 305; *J. Phys. Chem.* **1996**, *100*, 17873; *J. Phys. Chem. B* **1997**, *101*, 5506.
(12) Marky, N. L.; Manning, G. S. *J. Mol. Biol.* **1995**, *254*, 50.
(13) Mateescu, E. M.; Jeppesen, C.; Pincus, P. *Europhys. Lett.* **1999**, *46*, 493.
(14) Park, S. Y.; Bruinsma, R. F.; Gelbart, W. M. *Europhys. Lett.* **1999**, *46*, 454.
(15) Gurovitch, E.; Sens, P. *Phys. Rev. Lett.* **1999**, *82*, 339.
(16) Netz, R. R.; Joanny, J.-F. *Macromolecules* **1999**, *15*, 9013.
(17) Odijk, T. *Macromolecules* **1980**, *13*, 1542.
(18) von Goeler, F.; Muthukumar, M. *J. Chem. Phys.* **1994**, *100*, 7796. Haronska, P.; Vilgis, T. A.; Grottenmüller, R.; Schmidt, M. *Macromol. Theory Simul.* **1998**, *7*, 241.
(19) Verwey, E. J. W.; Overbeek, J. Th. G. *Theory of the Stability of Lyophobic Colloids*; Elsevier: Amsterdam, New York, 1948.
(20) Barrat, J.-L.; Joanny, J.-F. *Europhys. Lett.* **1993**, *24*, 333.
(21) Barrat, J.-L.; Joanny, J.-F. *J. Phys. II Fr.* **1994** , *4*, 1089.
(22) Kunze, K. K.; Netz, R. R. To be published.
(23) Borochov, N.; Eisenberg, H.; Kam, Z. *Biopolymers* **1981**, *20*, 231. Manning, G. S. *Biopolymers* **1981**, *20*, 1751.
(24) Odijk, T. *Langmuir* **1991**, *7*, 1991.
(25) Manning, G. S.; Ebralidse, K. K.; Mirzabekov, A. D.; Rich, A. *J. Biomol. Struct. Dyn.* **1989**, *6*, 877.

MA990264+